Supporting Information

Green and efficient graphitization of biomass waste empowered by molten salt electrolysis: Mechanistic exploration and energy storage applications dual-driven by experiments and simulations

Hailan Zhao,[a] Hao Wu,[a] Tao Rong,[a] Jun Zhao,[b] Mingyong Wang,[a] Shuqiang Jiao,*[ac] Haibin Zuo*[a]

H. Zhao, H. Wu, T. Rong, J. Zhao, Prof. M. Wang, Prof. S. Jiao, Prof. H. Zuo

[a] State Key Laboratory of Advanced Metallurgy, University of Science and Technology Beijing, Beijing 100083, Beijing, China.

[b] China Academy of Safety Science and Technology, Beijing 100012, China.

[c] School of materials science and Engineering, LanZhou University of Technology, Lanzhou 730050, Gansu, P. R. China.

E-mail: sjiao@ustb.edu.cn; zuohaibin@ustb.edu.cn

1 Experimental section

1.1 Preparation of carbon-containing precursor (WB)

3g of woody raw material (e.g., wood branches and wood chips) was pulverized and placed in a horizontal furnace. The temperature was slowly increased (10 °C/min) to 700 °C under Ar atmosphere, followed by high-temperature carbonization for 2 h to obtain fluffy carbon-containing precursors. The products were collected and used as cathode materials for subsequent electrolysis experiments.

1.2 Molten salt electrochemical conversion of WB

The synthesized WB powder (~1 g) was pressed into a cylinder with a diameter of 1.5 cm and a thickness of 0.5 cm under a pressure of 20 MPa. Then, the cylinder was wrapped with 400 mesh stainless steel mesh and wound with stainless steel wire (d = 1 mm). Finally, it was connected to an electrode rod to form the cathode. A high purity graphite rod (d=5 mm) was used for the anode.

Firstly, an alumina crucible (internal diameter of 70 mm, height of 120 mm) containing 200 g of anhydrous $CaCl_2$ was placed in a vertical closed tubular shaft furnace (SKL10-BY, Yunjie, Baotou, China) equipped with a programmable system. Then, it was dried at 400 °C for 6 h in a vacuum environment to remove water and impurities from the molten salt, and subsequently heated up to the target temperature (800-950 °C) under Ar atmosphere. The two electrodes were immersed in the molten salt after stabilization at the target temperature for 1h. Constant pressure electrolysis was performed between the WB cathode and graphite anode using an electrochemical workstation Versa STAT 3 (Princeton Center for Applied Research, USA). At the end of the reaction, both electrodes were lifted to the top position of the reactor and removed after cooling to room temperature in Ar. Finally, the electrolysis product (EGW) was obtained by repeated washing with 1 M dilute hydrochloric acid and deionized water as well as drying treatment at 80 °C.

1.3 Characterization

The changes in the crystal structure of the samples before and after electrolysis were analyzed by X-ray diffractometer (XRD, Rigaku Ultimate IV, Japan), and related parameters such as G were calculated. A Raman spectrometer (excitation wavelength of 532 nm) with a model of LabRAM HR Evolution was used to characterize the WB and the electrolysis products, and the molecular structure and chemical composition of the materials were analyzed in detail. XPS energy spectra were obtained by an X-ray photoelectron spectroscopy analyzer (Thermo Fisher 250xi) and used to analyze the chemical bonding and elemental composition of the sample surface. The micro-morphology and structure of WB and EGW were characterized by scanning electron microscopy (SEM, AJSM-F100) and transmission electron microscopy (TEM, JEM F200). FTIR spectra were obtained by a Fourier transform infrared spectrometer (Thermo Fisher IS5) to analyze the chemical composition and functional group types of the samples. Changes in the conventional organic element content of the samples before and after electrolysis were measured by an organic element analyzer (EA, FlashEA-1112). A specific surface and porosity analyzer (BET, Mike 2020) was used to determine the specific surface area and pore size of WB and EGW. The pore structure characteristics and changes of the materials were analyzed by plotting the N_2 adsorption/desorption isotherm.

1.4 Model construction and simulation calculations

To explore the potential forms of heteroatom removal in the molten salt electrolysis graphitization process, six simplified models were constructed using the Materials studio 2019 software, and the calculations and analyses of free energy and electrostatic potential were carried out. Given the complex surface structure and high molecular weight of WB molecules, which will bring higher computational difficulty as well as longer computation time for high-precision molecular simulation calculations. Therefore, in this study, we extracted the structural fragments of different functional groups containing heteroatoms in WB as computational objects to explore the ways of heteroatom removal in the graphitization transition.

Firstly, six representative functional group structures containing different heteroatoms were constructed using the visualizer tool in the Materials studio 2019 software. Before starting the calculations, electron density and electrostatics in the properties option bar were selected. The lowest energy configurations obtained after geometry optimization are noted as R-O, R-OH, R-NH, R-NH_2, R-S, and R-SH. The gray, white, red, blue, and yellow spheres in the constructed model represent carbon, hydrogen, oxygen, nitrogen, and sulfur atoms, respectively.

The energy of the models was calculated using the DMol3 module in the Materials studio 2019 software. The exchange-correction potential function was processed through the generalized gradient approximation (GGA) with the spin-polarized functional of Perdew-Burke-Emzerh (PBE).[1] The wave functions were expanded in a plane wave basis using a projector augmented wave (PAW) method and the energy cutoff was set to 400 eV. The structures were considered to be relaxed when all the forces on each ion were less than 0.02 eV/eV and the convergence criterion for the energies was 10^{-5} eV. To increase the effect of weak interactions on the system, we also performed van der Waals corrections. The free energy changes during the reduction reaction of O, N, and S heteroatoms under cathodic polarization were calculated by the following equation[2]

$$\Delta G_{ads} = \Delta E_{ads} - T\Delta S_{ads} + \Delta E_{ZPE}$$

Where ΔE_{ads}, ΔS_{ads}, and ΔE_{ZPE} are the energy change, reaction entropy change correction, and zero-point energy, respectively.

1.5 Electrochemical testing

The assembled CR2032 button cell was used to test the electrochemical properties of the electrolytic samples as a way to evaluate their actual performance in the battery.Therein, the working electrode was prepared as follows: firstly, EGW, carbon black, and polyvinylidene fluoride (PVDF) were mixed according to a mass ratio of 8:1:1, and subsequently dispersed in N-methyl-2-pyrrolidone (NMP) solvent with continuous stirring for 12h. Then, the uniformly mixed slurry was coated on the copper foil and dried at 60°C for 12h in vacuum oven. Finally, the treated copper foil was cut into electrode sheets with a diameter of 12 mm, and the loading of the active substance in the electrode was ~0.44 mg/cm^2. The lithium metal was used as counter electrode, and a polypropylene microporous membrane (Celgard 2500) was used as a diaphragm to prevent short-circuiting of the battery. 1 M $LiPF_6$ in ethylene carbonate (EC) and dimethyl carbonate (DEC) (1:1, v/v) with 5 wt% fluoroethylene carbonate (FEC) was used as the electrolyte. The assembly of the half-cells was performed entirely in an argon glove box ([O_2] < 0.1 ppm, [H_2O] < 0.1 ppm). Cyclic voltammetry (CV) curves of the half-cells were tested using an electrochemical workstation (VersaSTAT3, USA) with a set voltage window of 0.01-2V and a scan rate of 0.5 mV/s. A multi-channel battery test system (Neware CT-4008 T, China) was used to evaluate the constant-current charging/discharging performance of all the half-cells in the voltage range of 0.01-2V.

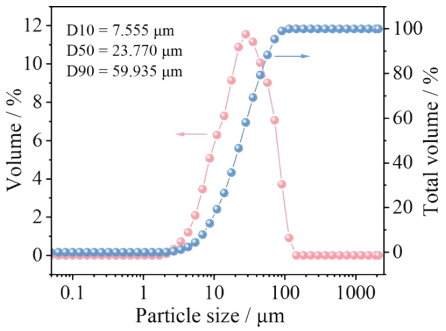

Fig. S1 The particle size distribution of WB

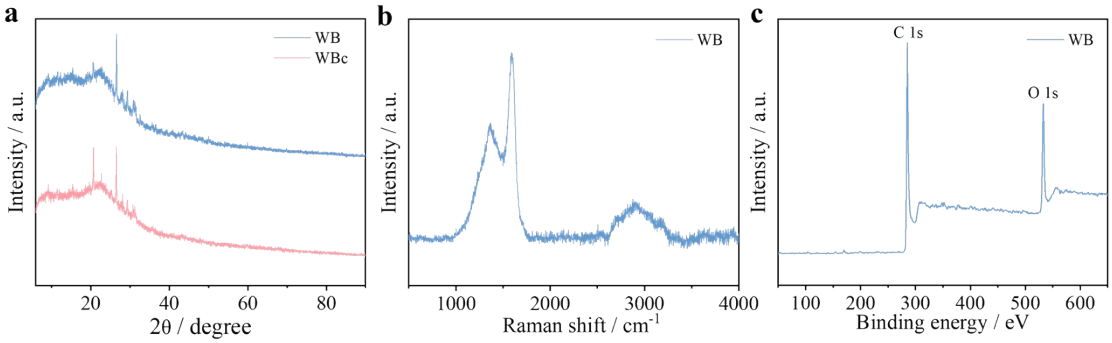

Fig. S2 (a) The XRD patterns of WB and control group (WBc); (b) The Raman pattern of WB; (c) The XPS pattern of WB.

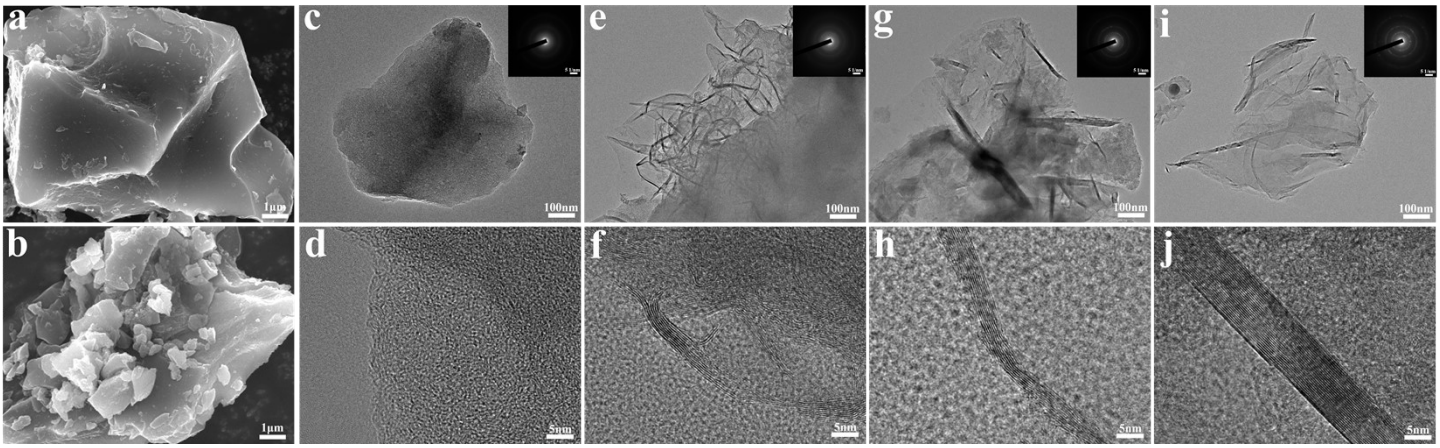

Fig. S3 SEM images of WB (a) and WBc (b). (c-j) TEM images of electrolysis samples obtained under different temperatures: (c-d) 800 °C, (e-f) 850 °C, (g-h) 900 °C and (i-j) 1000 °C at 2.6 V for 6 h.

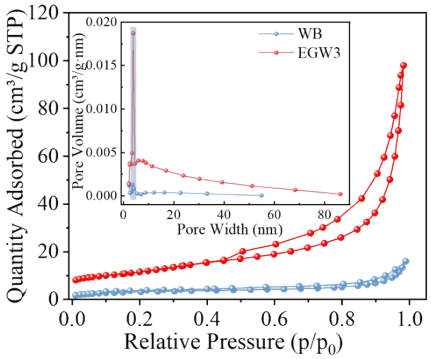

Fig. S4 N_2 adsorption-desorption curves of WB and EGW3.

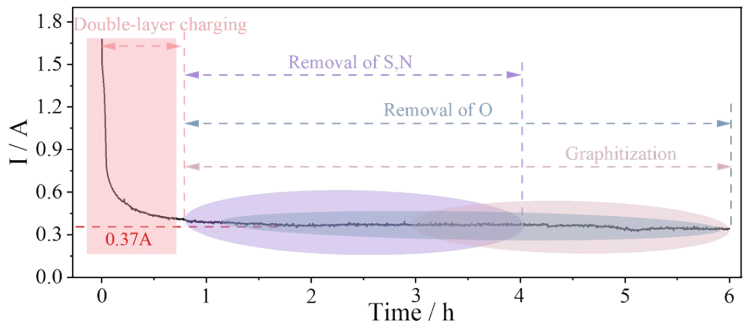

Fig. S5 Typical current-time response curve obtained under 950 °C and 2.6 V.

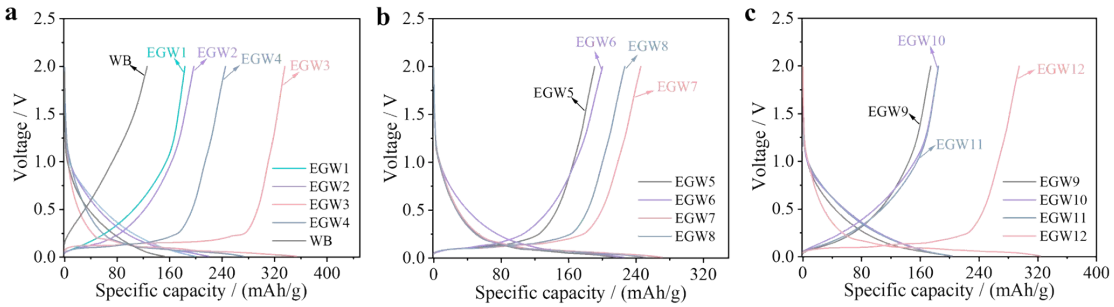

Fig. S6 The 2nd charge-discharge curves of WB and EGW obtained under different conditions at 1C. (a) different voltage; (b) different time; (c) different temperature.

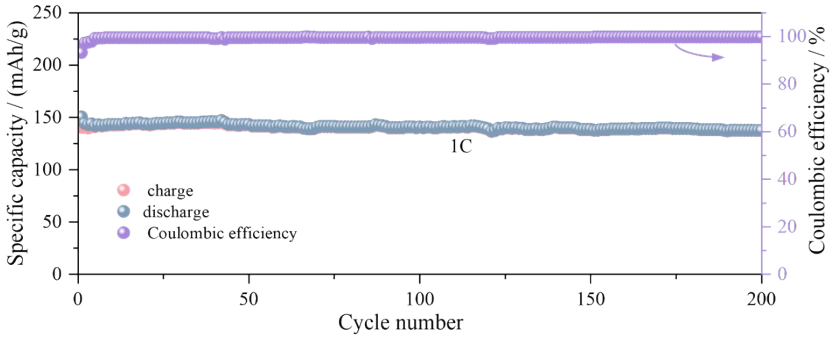

Fig. S7 Cycling stability and coulombic efficiency of the EGW3|$LiPF_6$+EC+DEC+FEC|$LiFePO_4$ full cells at 1 C.

Table S1 The composition of WB

Proximate analysis (wt%)				Ultimate analysis (wt%, daf)				impurity element (wt%)					
M_{ad}	A_{ad}	V_{daf}	FC_{ad}	C	O	N	S	Ca	K	Mg	Na	Fe	Si
7.24	10.27	31.79	53.00	63.435	20.627	0.774	1.249	1.02	1.81	0.22	0.26	0.28	1.66

M_{ad} is the moisture content on air-dried basis, A_{ad} is the ash content on air-dried basis, V_{daf} is the volatile matter content on a dry, ash-free basis, FC_{ad} stands for fixed carbon.

Table S2 The graphitization degree of WB and the samples obtained under various electrolysis conditions.

Samples	2θ / °	FWHM / °	d_{002} / Å	Lc / nm	N / -	G / %
WB	25.17	12.37	0.3535	0.66	1.86	-110.80
EGW1	25.84	7.90	0.3445	1.03	2.99	-5.96
EGW2	26.29	0.63	0.3387	12.92	38.15	61.43
EGW3	26.40	0.61	0.3373	13.40	39.71	77.56
EGW4	26.40	0.58	0.3373	14.19	42.06	77.56
EGW5	26.18	1.33	0.3401	6.15	18.08	45.18
EGW6	26.19	1.00	0.3400	8.18	24.05	46.66
EGW7	26.40	0.61	0.3373	13.40	39.71	77.56
EGW8	26.42	0.60	0.3371	13.57	40.27	80.47
EGW9	25.94	7.43	0.3432	1.10	3.20	9.22
EGW10	26.13	6.59	0.3408	1.24	3.63	37.74
EGW11	26.36	0.68	0.3378	12.01	35.56	71.71
EGW12	26.48	0.60	0.3363	13.51	40.15	89.20

Table S3 The graphite yield after electrolysis under different conditions.

Samples	Electrolysis condition	Graphite yield / %
EGW1	950℃-**2.2V**-6h	60.07
EGW2	950℃-**2.4V**-6h	58.89
EGW3	950℃-**2.6V**-6h	58.40
EGW4	950℃-**2.8V**-6h	30.37
EGW5	950℃-2.6V-**2h**	62.34
EGW6	950℃-2.6V-**4h**	58.47
EGW7	950℃-2.6V-**8h**	49.86
EGW8	950℃-2.6V-**10h**	44.47
EGW9	**800℃**-2.6V-6h	63.42
EGW10	**850℃**-2.6V-6h	57.82
EGW11	**900℃**-2.6V-6h	57.24
EGW12	**1000℃**-2.6V-6h	47.73

Table S4 The I_D/I_G values of the samples obtained under various electrolysis conditions.

Samples	D peak		G peak		I_D/I_G
	Position / cm^{-1}	FWHM / °	Position / cm^{-1}	FWHM / °	
WB	1352.26	227.57	1587.02	77.13	0.9306
EGW1	1346.32	127.41	1589.60	76.80	1.1396
EGW2	1344.25	99.40	1578.36	57.33	0.5989

EGW3	1350.30	55.42	1582.53	40.07	0.3005
EGW4	1351.82	44.34	1582.05	36.21	0.2854
EGW5	1343.41	139.70	1591.95	66.19	1.1765
EGW6	1349.25	48.82	1582.15	32.68	0.5045
EGW7	1346.94	43.68	1579.86	25.77	0.2671
EGW8	1350.88	43.35	1579.86	23.77	0.2350
EGW9	1338.09	195.09	1579.16	87.08	1.1217
EGW10	1344.47	150.47	1576.70	102.07	0.9854
EGW11	1348.43	78.64	1581.30	51.78	0.4258
EGW12	1349.83	67.61	1583.44	48.22	0.2841

Table S5 Chemical composition (atoms, %) of the samples' surfaces obtained by XPS spectra.

Samples	C / %	O / %	N / %	S / %
WB	80.02	17.74	1.55	0.69
EGW1	90.45	8.08	1.32	0.14
EGW2	92.31	6.54	1.03	0.11
EGW3	95.97	3.32	0.61	0.10
EGW4	95.98	3.31	0.60	0.11
EGW5	94.09	4.88	0.71	0.32
EGW6	95.05	3.99	0.68	0.27
EGW7	96.01	3.31	0.58	0.10
EGW8	96.07	3.28	0.56	0.09
EGW9	90.18	8.13	0.98	0.71
EGW10	91.44	7.56	0.65	0.36
EGW11	93.19	5.91	0.66	0.24
EGW12	95.99	3.30	0.62	0.09

Table S6 Physical properties of WB and EGW3 obtained from BET tests.

Samples	Conditions	BET surface area (m^2/g)	Average pore diameter (nm)
WB	Woody Biochar	11.6204	8.5453
EGW3	950℃-2.6V-6h	41.2000	14.7195

Table S7 The elemental contents in WB and the samples obtained under various electrolysis times measured by EA.

Samples	C / %	O / %	N / %	S / %
WB	63.435	20.627	0.774	1.249
EGW5	65.463	2.358	0.162	0.069
EGW6	72.514	2.326	0.153	0.063
EGW3	80.881	1.400	0.074	0.048

EGW7	81.300	1.223	0.073	0.036
EGW8	80.970	1.220	0.067	0.029

Table S8 The charge-discharge capacities and coulombic efficiencies of samples at 1C for the second cycle.

Samples	Discharge capacity (mA h/g)	Charge capacity (mA h/g)	Irreversible capacity (mA h/g)	Coulombic efficiency (%)
WB	151.89	125.83	26.06	82.84
EGW1	200.44	179.70	20.74	89.65
EGW2	219.63	196.93	22.70	89.66
EGW3	353.31	335.61	17.70	94.99
EGW4	272.41	245.22	27.19	90.02
EGW5	215.54	190.94	24.60	88.59
EGW6	225.72	200.38	25.34	88.77
EGW7	271.11	245.67	25.44	90.62
EGW8	250.34	226.67	23.67	90.54
EGW9	201.82	174.27	27.55	86.35
EGW10	203.43	184.52	18.91	90.70
EGW11	203.18	184.83	18.35	90.97
EGW12	323.66	294.85	28.81	91.10

References

1 J. P. Perdew, K. Burke and M. Ernzerhof, *Phys. Rev. Lett.*, 1996, **77**, 3865.
2 S. Zhang, Z.-Q. Huang, Y. Ma, W. Gao, J. Li, F. Cao, et al., *Nat. Commun.*, 2017, **8**, 15266.